NRIAG JOURNAL OF ASTRONOMY AND GEOPHYSICS
2022, VOL. 11, NO. 1, 1–20
https://doi.org/10.1080/20909977.2021.2020999

Geoelectric characterisation of furnace and slag trench structures: Case study Obafemi Awolowo University ancient iron smelting site, Ile-Ife, southwest Nigeria

Martins Olusola Olorunfemi, Ademakinwa George Oni and Taiwo Kazeem Fadare

Department of Geology, Obafemi Awolowo University, Ile-Ife, Nigeria

ABSTRACT

We utilised resisto-thermal effect of iron smelting to precisely locate concealed furnaces and slag trenches at an ancient iron smelting site situated within the estate of Obafemi Awolowo University, Ile-Ife, Southwest Nigeria. The methodology involved closely spaced, small electrode spacing (micro) Vertical Electrical Soundings across diagnostic dipolar magnetic anomaly closures. Both the furnace and the slag trench sites were characterised by thermal induced enhanced layer resistivity values and anomalously high depth extent of an index (second) resisto-archaeological geoelectric layer with higher influence beneath the furnace than the slag trench. The results showed that the location of the furnace is shifted from the centre of the magnetic low (negative), sometimes overlapping the transition zone towards the magnetic high (positive) while the slag trench is generally situated within the magnetic high zone. Preliminary archaeological excavation at one of the investigated sites (site 1) identified a furnace and the adjoining slag trench structures at the precise locations predicted from the geoelectric section. The study concluded that thermal-induced resistivity attribute is effective in precisely locating concealed ancient iron smelting furnace and slag trench structures.

ARTICLE HISTORY
Received 10 May 2021
Revised 11 November 2021
Accepted 16 December 2021

KEYWORDS
Geoelectric characterisation; resisto-thermal effect; iron smelting; furnace/slag trench structure delineation

1. Introduction

Iron smelting sites are usually situated close to or within network of water channels, near the headwaters of small and large streams or in the premises of the confluence of two streams (de Barros 2000). The sites are moderate in size and usually contain two to three mounds and sometimes up to 15 mounds with average height of 0.8 m but rarely higher than 1.5 m and lengths of 10–12 m and sometimes up to 20 m (de Barros 2000). According to the referenced author, iron smelting sites are typically compounds of between 1 and 4 or 5 groups of mounds with typically one furnace per group. Ratio of furnace emplacement to mounds lies between 1:2 or 1:3 and often times two or more smelting teams often work at the same location. Furnaces and iron slag trenches are primary components of an ancient iron smelting site structure.

Iron smelting furnace architecture and characteristics vary with regions and localities. Furnaces could be cylindrical, circular, rectangular and sometimes oval in shape (Ige and Rehren 2003; Akinjogbin 2004; Holl 2009; Kozhevnikov et al. 2018) founded on hard and properly drained ground and built on raised platforms. The diameter ranges from 0.65 to 2.0 m with heights of between 1.7 and 7.0 m and bottom depth extent of 0.46–0.61 m (Adeniji 1977; Childs 2000; Ige and Rehren 2003; Akinjogbin 2004; jemkur 2004; Holl 2009; Kozhevnikov et al. 2018) and wall thickness of 0.045–0.07 m (Ige and Rehren 2003; Holl 2009). The furnace wall is built with clay or mud and sometimes coated with thin red fire-hardened bricks (Ige and Rehren 2003; Holl 2009). According to Adeniji (1977) and Akinjogbin (2004), a typical iron smelting furnace in Yorubaland in southwest Nigeria contains two slag trenches with the smaller and shallower one dug facing the eastern entrance and ending up at the base of the furnace platform while the bigger and deeper trench (sometimes up to 3 × 3 × 3 m) is dug facing the west entrance and is connected to the centre of the furnace through which hot air escapes the furnace and slag drops from the furnace into the large pit. Six openings are created at the base of the furnace with inserted tuyeres, which are connected with the east facing trench that regulate the inflow of fresh air.

A furnace site is therefore typified by the presence of slag, clay brick fragments, broken tuyeres, ash (grey/black), ash turned soils and pieces of charcoal within its inner part (de Barros 2000; Ige and Rehren 2003; Holl 2009; Kozhevnikov et al. 2018). The identification of the location of a furnace is problematic unless the baked (hardened) base is found in situ (in place). In most places where iron smelting had been carried out, some of which are now within urban areas, furnaces have been destroyed as a result of infrastructural development, or mechanised agricultural practice. This has made direct location of ancient furnace sites

CONTACT Ademakinwa George Oni oniademakinwa@yahoo.com Department of Geology, Obafemi Awolowo University, Ile-Ife, Nigeria

very difficult, if not impossible. Furnaces are known to be fired to temperatures well above 1000°C and sometimes up to 1536°C (Okafor 2002; Deme and McIntosh 2006; Fluzin 2007; Holl 2009) that is well above the curie point temperature (550°C) of most rocks at which earth materials lose ability to retain magnetism (that is changes from ferromagnetic to paramagnetic behaviour). When the furnace cools below the curie point temperature, thermo-remanent magnetisation is acquired (Powell et al. 2002). Iron smelting therefore enables the furnace wall lining, in-fill and its immediate environment to acquire higher magnetic susceptibility relative to the host and this could aid its delineation. The heating process also leads to hardening through baking of both the base and the furnace wall, slag trench wall including its immediate environment (Kozhevnikov et al. 2018) thereby leading to lower moisture content, reduced porosity and higher resistivity.

Due to the confined nature of the heat within the furnace, its influence is expected to be deeper directly beneath the furnace bottom and decreases outwards. These magnetic and resistivity attributes of iron smelting site can be used to indirectly locate both furnace and slag trench sites (e.g. Powell et al. 2002).

The Obafemi Awolowo University (OAU) iron smelting site, situated in Ile-Ife, Osun State, Southwest Nigeria (Figure 1), has the characteristic features of an ancient iron smelting site including varieties of iron slags, pieces of tuyere, fragments of fired furnace wall, iron nodules and mounds (Figure 2). However, the only physical evidence of its furnace(s) is in scattered pieces of fired clay suspected to be relics of the furnace wall. The geophysical characterisation of the ancient smelting site by Olorunfemi et al. (2021) involved integrated magnetic and electrical resistivity methods. Three sites (1, 2 and 3) (Figure 1) with dipolar (circular/oval-shape) magnetic anomalies with high amplitude (negative polarity in the low magnetic latitude region) closure over suspected furnace structure and an adjoining lower or higher amplitude (positive polarity) closure over the slag (gangue) trench, as observed by Powell et al. (2002) were identified. The resistivity attributes (maps) were not distinctly diagnostic with conflicting low and high resistivity anomalies obtained over suspected furnace and slag structures. Table 1 displays the recommended sites for follow-up archaeological excavation and the magnetic and resistivity attributes for two of the three identified sites.

The magnetic response of an iron smelting site is an integration of the responses from the magnetic anomalies associated with its furnace and associated structures, slag deposit and the underlying and surrounding geology of the site (Powell et al. 2002). This means that the geometries/sizes of the magnetic anomalies will be much larger than the causative bodies, including the furnace. Locations of furnaces

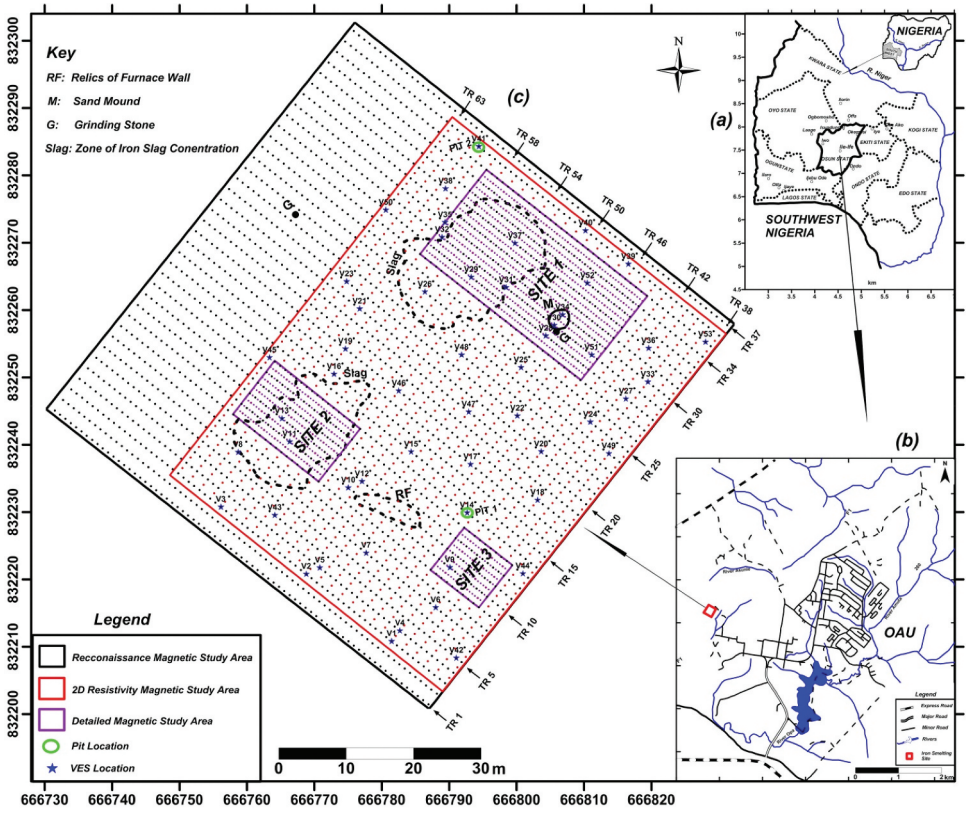

Figure 1. Location and data acquisition map of the study area (a) map of southwest Nigeria with Nigeria as inset (b) map of OAU campus showing the study area (c) field layout at OAU archaeological site.

Figure 2. OAU iron smelting site showing (a) iron slag (b) broken fired tuyere (c) piece of fired clay furnace wall (d) iron nodules (e) boulders of quartz (rock stones) of different sizes and shapes (f) mound.

Table 1. Geophysical characteristics of sites recommended for follow-up archaeological excavation (culled Olorunfemi et al. 2021).

Serial No.	Site	Magnetic/Resistivity Anomalies	Magnetic/Resistivity Characteristics	Suspected Archaeological Features
1	1	A_1	Magnetic Low (-ve) closure/Low & High Resistivity Anomaly	Furnace Structure
2		A_2	Magnetic Low (-ve) closure/Low Resistivity Anomaly	Furnace Structure
3		A_3	Magnetic High (+ve) closure/High Resistivity Anomaly	Slag Trench
4		B_1	Magnetic Low (-ve) closure/Low Resistivity Anomaly	Furnace Structure
5		B_2	Magnetic High (+ve) closure/Low Resistivity Anomaly	Slag Trench
6		B_4	Magnetic High (+ve) Rectangular closure/Low Resistivity Anomaly	Structure Foundation
7	2	C_1	Magnetic Low (-ve) closure/High Resistivity Anomaly	Furnace Structure
8		C_2	Magnetic High (-ve) closure/High Very High Resistivity Anomaly	Slag Trench

(kilns) are also known to be shifted from the centres of the magnetic anomalies (Abrahamsen et al. (1984) and Pattantyús-Á (1986) in Sharma (1997) and Powell et al. (2002)). Pattantyús-Á (1986) attributed this to inclination of magnetisation vectors.

The main objective of the present study, therefore, is to develop a methodology for precise location of iron smelting furnace and its associated slag trench site using the thermal induced enhanced resistivity effect. Since our interest is in vertical variations in the subsoil resistivity and at relatively shallow depth (<15 m) small (micro)-electrode spacing Vertical Electrical (resistivity) Sounding (VES) technique was adopted.

2. Methodology

A traverse was established through the centre and normal to the trend of prominent bipolar magnetic anomaly along which micro Vertical Electrical Soundings (VES) was carried out at intervals of 0.5 m. The micro-VES utilised the Schlumberger array with half potential electrode spacing (MN/2) varying from 0.03 to 1.0 m and half current electrode spacing (AB/2) ranging from 0.075 to 15 m (Figure 3). The depth sounding was carried out by gradually expanding the electrode spacings relative to the centre of the electrode array (Telford et al. 1990; Reynolds 1997). The apparent resistivity values were computed from equation 1.

$$\rho_a = \pi \frac{\Delta V}{I} \frac{(AB/2)^2}{MN} \tag{1}$$

where AB/2 is half the current electrode spacing;
MN is potential electrode spacing;
ΔV is potential difference;
I is input current; and
π is a constant (22/7).
(Note $\frac{\Delta V}{I} = R$, the ground resistance)

The apparent resistivity values were plotted against half current electrode spacing (AB/2) and connected with smooth curves. The VES curves were quantitatively interpreted by partial curve matching and 1D forward modelling with W-Geosoft/Winsev version

Electrode Position	Half Current Spacing (m)	Half Potential Spacing (m)
	AB/2	MN/2
1	0.075	0.030
2	0.125	0.030
3	0.25	0.030
4	0.25	0.065
5	0.50	0.065
6	0.50	0.125
7	1.0	0.125
8	1.0	0.25
9	2.0	0.25
10	3.0	0.25
11	4.0	0.25
12	6.0	0.25
13	6.0	0.50
14	8.0	0.50
15	12.0	0.50
16	15.0	0.50
17	15.0	1.0

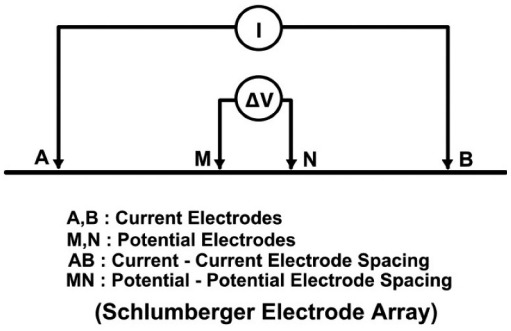

Figure 3. Electrode configuration for Schlumberger array micro (VES) sounding.

5.1 software. The final interpretation results were used to prepare a geoelectric section along the investigated traverse. A preliminary investigation involving this methodology was carried out at Iyekere, Ile-Ife, with established furnace and slag trench structures.

3. Results

3.1. Iyekere iron smelting site preliminary study

Iyekere, in Ile-Ife, is a renowned iron smelting community (Ige and Rehren 2003) with many iron smelting sites. Urban infrastructural development has obliterated many of the sites and destroyed its archaeological features. One of the prominent iron smelting site is located in the premises of Anglican Secondary Commercial Grammar School, Iyekere, Ile-Ife (Figure 4), where an earth road and construction works within the school have exposed one rectangular-shaped furnace site and relics of what looks like other sites with features typical of furnaces such as tuyere, fragments of clay furnace wall, iron slags, black soil residue (ash) and pottery fragments (Figure 5(a–c); Oyeyemi et al. 2015). It is very rare to find exposed iron smelting furnace, which makes the site suitable for the preliminary study of the thermally induced enhanced resistivity effect of furnacing.

Prior to the geoelectric investigation, a reconnaissan ce total field magnetic survey was carried out along six traverses (spaced at 2 m interval) with station interval of 1 m to confirm exposed furnace structure/slag trench and identify concealed ones. The magnetic data, acquired with GSM-19 T Proton Precession Magnetometer, were corrected for diurnal variation and offset and subsequently reduced to the equator (RTE) to remove asymmetry and correctly locate magnetic anomalies over the causative bodies. The corrected magnetic data were plotted against stations along the occupied traverses and contoured.

Figure 6 presents the reduced to the equator (RTE) magnetic map. A dipolar magnetic anomaly (positive and negative magnetic closures) typical of an iron smelting furnace and its associated slag trench (Powell et al. 2002) was observed within the premises of the established prominent furnace site (site 1) with the furnace partly located within the transition zone between the magnetic high (positive) and low (negative) and significantly within the magnetic low region. Powell et al. (2002) established that the furnace site is shifted from the centre of the magnetic low. The magnetic map also identifies another prominent but partly bifurcated dipolar magnetic anomaly east of furnace site 1, around the school entrance steel structured gate and collapsed security post. This magnetic anomaly was suspected to have been partly created by the gate. However we observed several pieces of tuyere, baked clay fragments and black soils beneath the floor of the collapsed security post beside the gate (Figure 5c). While the furnace at site 1 gives diagnostic magnetic anomaly, other suspected furnaces at sites 2 and 3 (Figure 6) did not produce such diagnostic magnetic anomalies.

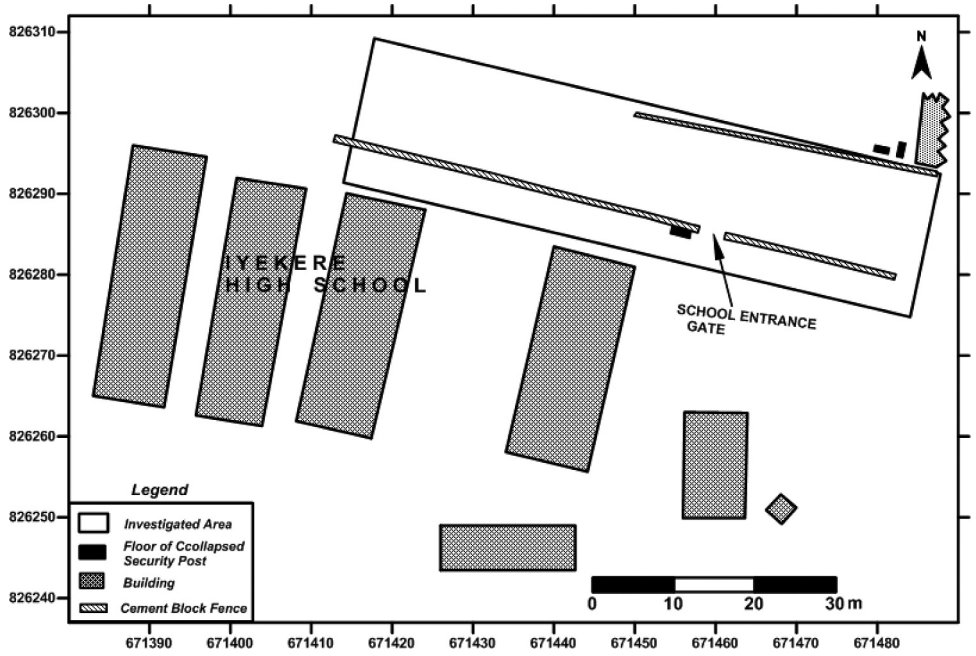

Figure 4. Site map of Iyekere iron smelting site showing the investigated area.

We carried out a follow-up twenty nine (29) micro-Vertical Electrical Soundings (VES) at 0.5 m interval along traverse TR5 that cut across the prominent dipolar magnetic anomalies at site 1 and the second magnetic low closure on its eastern side (Figure 6).

The typical VES curves are displayed in Figure 7 while the interpretation results are contained in Table A1 in the Appendix. The resistivity type curves range from four layer QQ type to five layer HAK, HKH, KHK, KQH, KQQ, six layer HKHK, KQHK, QHKH, KQQH and seven layer AKHKH, HKHKH, HKQKH and KHKHK type. The primary A, H, K, and Q type curves have resistivity combinations of $\rho_1 < \rho_2 < \rho_3$; $\rho_1 > \rho_2 < \rho_3$; $\rho_1 < \rho_2 > \rho_4$ and $\rho_1 > \rho_2 > \rho_3$ where ρ_1, ρ_2 and ρ_3 are the first-, second-, and third-layer resistivity values. The other multi–layered type curves with resistivity layer combinations greater than four layers are derived from these four primary three-layer resistivity type curves (Olorunfemi et al. 2021). The micro (small electrode spacing) VES delineated up to four micro-layers in the upper 1.0 m which in conventional VES (with starting current electrode spacing, AB/2 of 1.0 m) are lumped together as the topsoil. It also reflects the geoelectric complexity of the subsoil derived from the schist underlain area, at shallow depth.

The geoelectric section generated from the VES interpretation results in the upper 10 m and along the investigated traverse is displayed in Figure 8(a) (bottom). The first resisto-archaeological layer has resistivity values ranging from 82 to 1360 Ωm and thicknesses of between 0.06 and 0.78 m with the exception of beneath VES 1 and 2 with thicknesses of 1.3 m and 0.9 m, respectively. The thicknesses are generally less than 0.35 m (35 cm). This layer constitutes the topsoil and is composed of recent sediments including humus soil, clay/sandy clay and clayey sand/laterite. The heterogeneous nature of this layer explains the wide range of resistivity values. The surface/near-surface nature of this horizon, its near uniform thickness, and susceptibility to anthropogenic influence do not make it an index layer for assessment of the resisto-thermal influence. The second resisto-archaeological layer displays layer resistivity values that range from 33 to 181 Ωm and thicknesses of between 0.46 and 7.8 m. The near uniform resistivity value of the second horizon typifies clay/sandy clay layer while the significant variability in its depth extent could be related to heat effect. This horizon is thickest beneath the field observed furnace site (stations VES 8–12). This suspected heat impacted zone (between stations VES 9–12) overlaps significantly with the furnace location, whose centre could be around station 10.5. The depth extent of this horizon (about 4.4 m) beneath the field observed slag trench (between stations VES 4 and 6.5) is shallower than beneath the furnace (see Figure 8(a)). This is expected, in view of higher furnace temperature. Two additional resisto-thermal anomalous zones of about the same depth extent (6.1 and 6.4 m) were identified between stations VES 19 and 22 and 23 and 26. These anomalous zones are suspected to be two adjacent furnaces of about the same age but could be younger (with shallower depth extent) than that at site 1. These suspected furnaces must have been responsible for the bifurcated magnetic low (negative polarity) closures around the school gate (Figure 6). Further examination of the survey premises led to the identification of broken tuyeres beneath the floor of the collapsed security

Figure 5. (a) Iyekere, Ile-Ife iron smelting site showing a rectangular-shape furnace. (b) Circular-shape furnace site at Iyekere, Ile-Ife irom smelting site showing iron slag, broken tuyere and fired clay. (c) Suspected furnace beneath the floor of collapsed security post by the side of the school entrance gate with tuyere pipes in place and pieces of iron slag at Iyekere, Ile-Ife ancient iron smelting site.

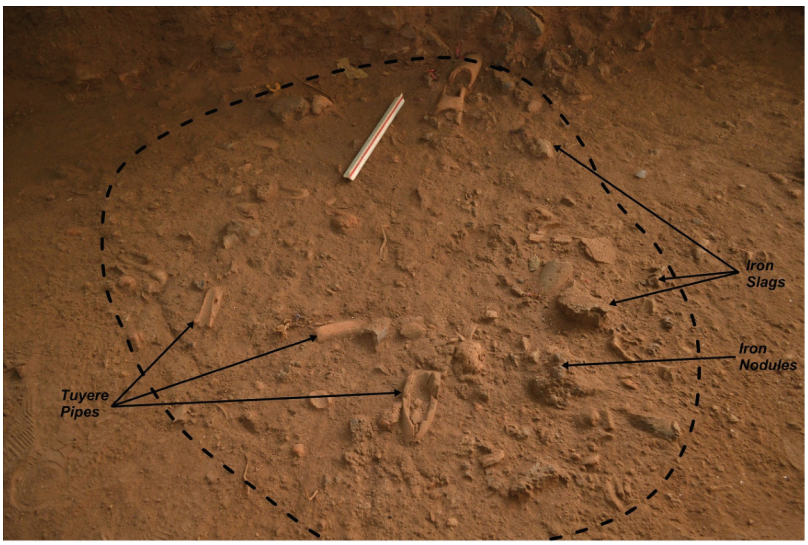

Figure 5. Continued.

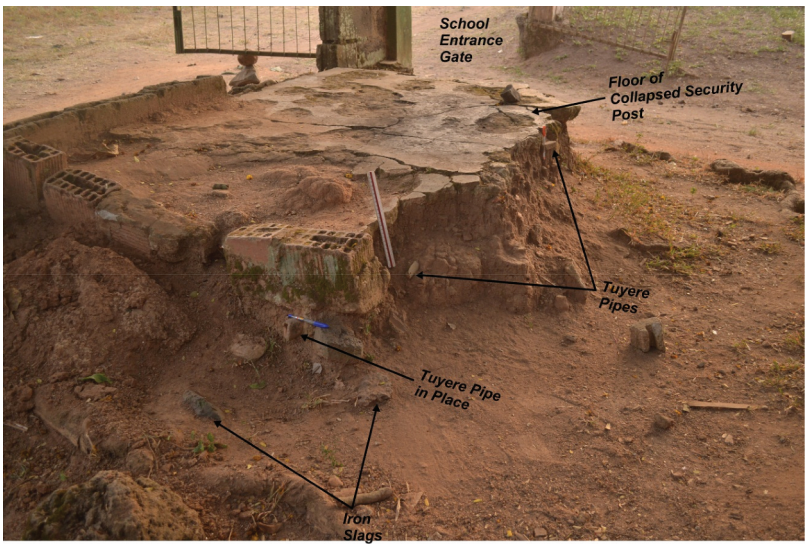

Figure 5. Continued.

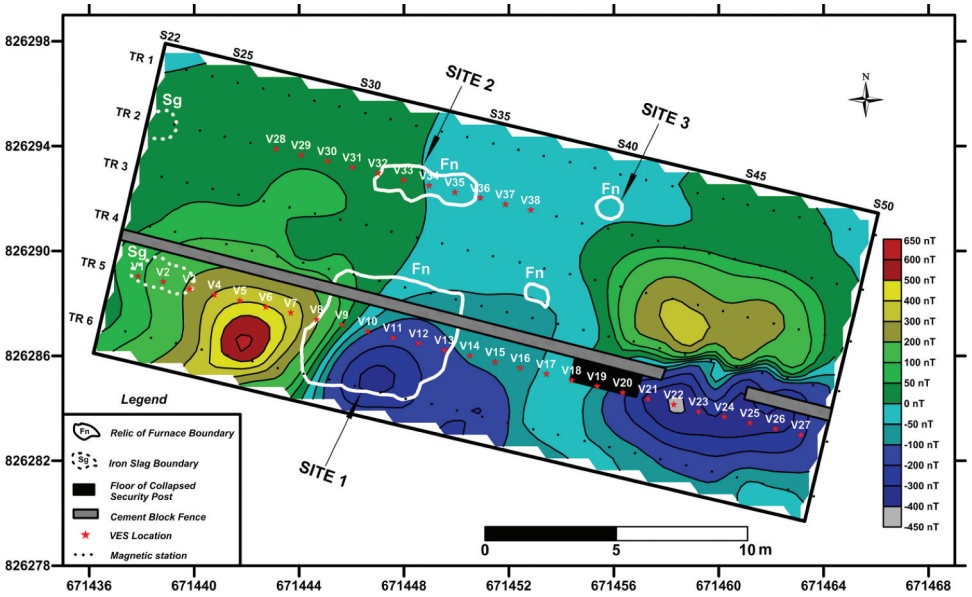

Figure 6. Reduced to the equator magnetic (RTE) map showing the micro VES locations.

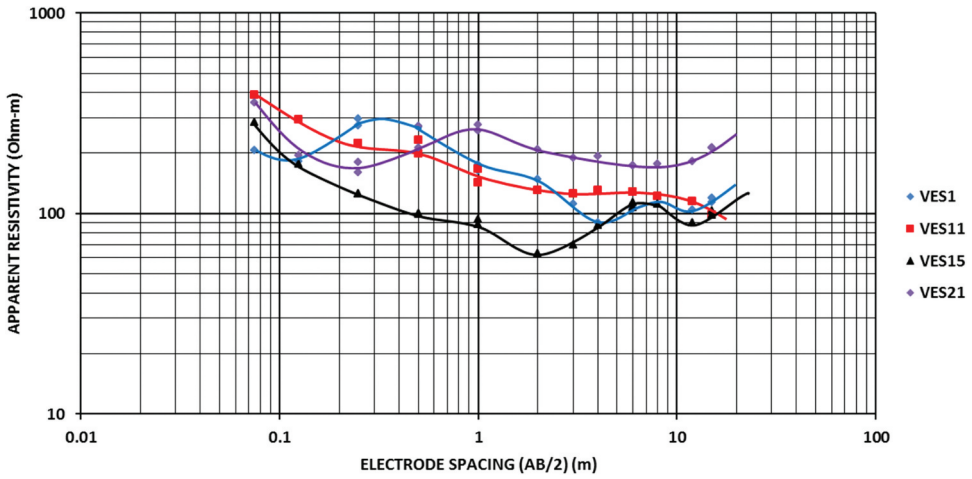

Figure 7. Typical VES curves at Iyekere iron smelting site.

post by the school gate (Figure 5(c)) around stations VES 19–21. Ancient iron smelting site are known to contain many furnaces (de Barros 2000).

The correlation of an established furnace and slag trench sites with zones having thickest depth extents (larger for the former) of the second resisto-archaeological layer makes this layer a resisto-thermal index horizon and will hence-forth be so referred. The third geoelectric layer has layer resistivity values that range between 81 and 570 Ωm (but generally >135 Ωm) typical of clay/sandy clay and clayey sand with thicknesses varying from 0.8 to 4.4 m, where the bottom interface was delineated. The fourth layer has layer resistivity values of between 16 and 129 Ωm (but generally <100 Ωm) characteristic of clay with depth to top of 1.8–10 m, where the upper interface is delineated (Figure 8(a)). These two bottom layers are of no archaeological interest.

Super-imposed on the geoelectric section is a resistivity profile for the index horizon (second resisto-archaeological layer) (Figure 8(b)). The resistivity profile shows that the layer resistivity values are slightly higher (peaks) over both the furnaces and iron slag trenches (compare Figure 8(a–b)).

The following are deductions from the Iyekere case study.

(i) Enhanced layer resistivity values and depth extents of index (second resisto-archaeological) layer are characteristics of the thermal effect of iron smelting furnace and slag trench.

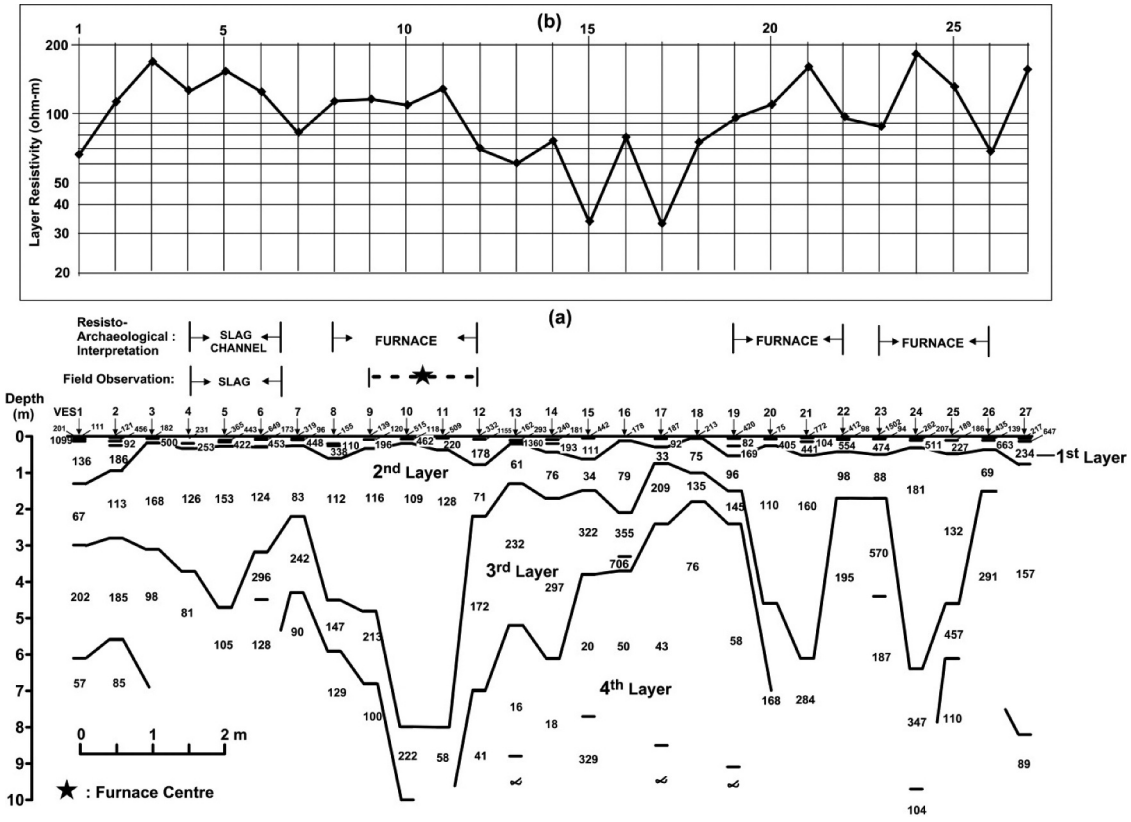

Figure 8. (a) Geoelectric section across Iyekere iron smelting furnaces and (b) resistivity profile of the index second resisto-archaeological layer.

(ii) The depth extent (of the thermal influence on the layer resistivity) beneath the furnace is greater than beneath the iron slag trench while resistivity profile of the index layer peaks above both the furnace and slag trench.
(iii) The depth extent of the index second layer peaks at around the centre of the furnace and slag trench.
(iv) Where multiple furnaces exist, the depth extent could be used to establish the relative age of the furnaces with older furnaces having greater depth extent of the thermal influence.

3.2. OAU iron smelting site study

In Table 1, four furnace structures were suspected to be situated within the investigated OAU iron smelting site and typified by magnetic low (negative) anomalous zones A_1, A_2, B_1 at site 1 and C_1 at site 2 with their associated slag trenches displaying magnetic high (positive) anomalous zones A_3, A_4, B_2, and C_2 (Figure 9).

Figure 10(a-c) shows isolated magnetic anomalous zones A and B (site 1) and C (site 2) with superimposed micro-VES investigated axes and stations. The anomalous zones were further investigated for precise location of furnaces/iron slag trenches based on deductions from the Iyereke case study. The same methodology (detailed above) adopted at the Iyekere, Ile-Ife, iron smelting site, was applied. Investigated profiles were established approximately normal to the trends of the magnetic anomalous zones. The investigated sites are underlain by grey gneiss basement rock.

The micro-VES interpretation results are contained in Tables A2–A4 (in the Appendix). Except for VES stations 19, 22 and 23 which display KHA resistivity type curve, all the remaining 82 (96%) VES curves are of the KH type (Figure 11). The near–surface subsoils are generally uniform at the OAU, Ile-Ife, grey gneiss underlain iron smelting site as against the Iyekere, schist underlain locality (compare Figures 7 and 11).

3.2.1. Site 1 magnetic anomalous zone A

Figure 12(a) shows the geoelectric section generated across magnetic anomalous zone A (A_1, A_2, A_3 and A_4). The high amplitude negative polarity anomaly closures A_1 and A_2 were interpreted based on Powell et al. (2002), as suspected furnaces while the high amplitude positive polarity anomaly closures A_3 and A_4, as possible iron slag channels.

Three resisto-archaeological layers were delineated by the geoelectric section. The first layer is generally composed of upper two geoelectric layers with resistivity values ranging from 38to 2032 Ωm and thicknesses

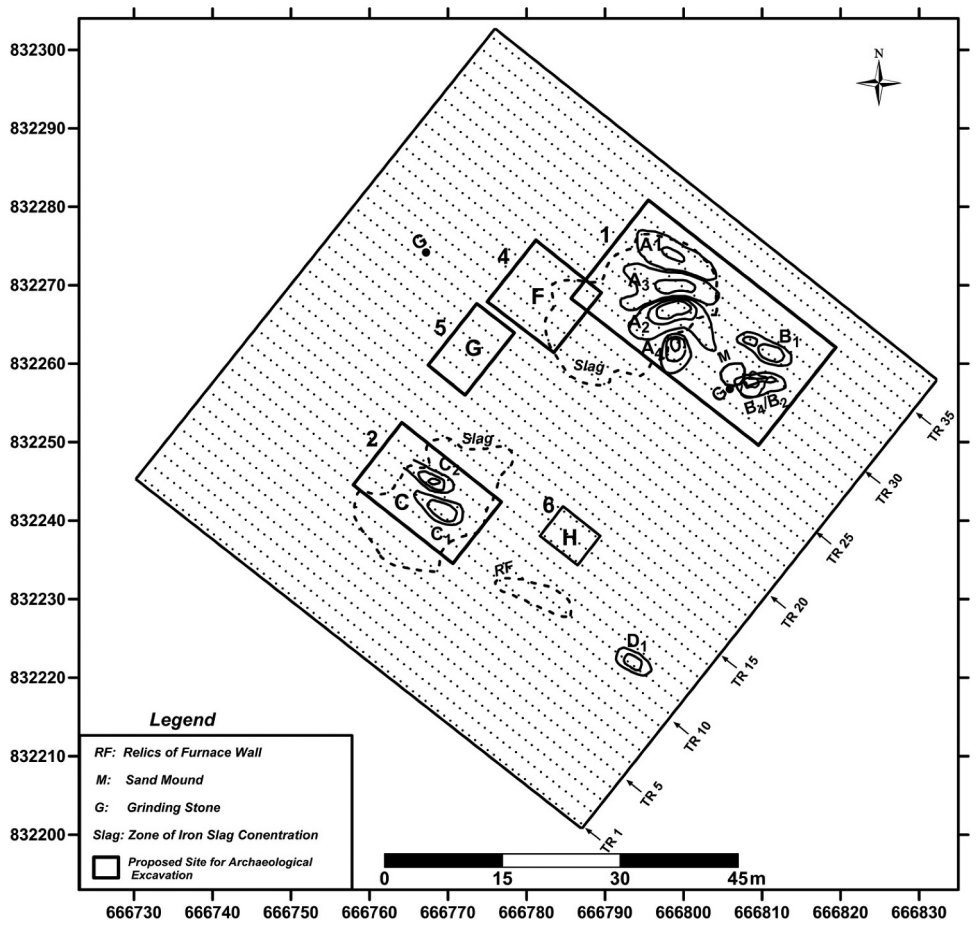

Figure 9. Map showing proposed sites for archaeological excavation with superimposed magnetic anomaly outlines (Olorunfemi et al. 2021).

of between 0.06 and 0.86 m but generally < 0.50 m (50 cm). This horizon is composed of humus soil, clay, sandy clay, clayey sand and laterite. Except beneath VES 2, 27 and 28, the thicknesses are generally uniform.

The second (and the index) resisto-archaeological layer has layer resistivity values of between 111 and 393 Ωm (Figure 12(a–b)) with thicknesses of between 0.53 and 12.86 m. The layer resistivity is generally uniform and typical of sandy clay. The layer thicknesses, as observed at Iyekere, Ile-Ife, are variable and thickest beneath the suspected furnace site. The third layer has resistivity values of between 258 and ∞ Ωm with depth to bedrock of between 0.7 and 13 m.

The resistivity of the index layer (Figure 12(b)) shows eight peaks. Peak P_6, is located at the centre of zone VES 22–26 where the index second layer has the highest depth of 13 m. This zone, based on the Iyekere case study, is suspected to host a furnace (F_1) whose centre is located beneath around VES 24. The anomalous zone VES 18–21 adjoining F_1 to the north is suspected to be a slag channel (S_1) beneath, which the index horizon has a shallower depth extent of 8.3 m. The resistivity peak P_5, at VES 19 is suspected to be about the centre of the slag trench. The location of suspected furnace F_1, is shifted from the centre of the negative magnetic anomaly closure A_2 and slightly northwards and straddles into the southern edge of the positive magnetic anomaly closure A_3. The suspected slag trench S_1 is located within the northern edge of the anomaly closure A_3. Resistivity peaks P_7 and P_8 are located at the centres of zones VES 30–34 and VES 34–37 with fairly thick index second layer (maxima of 4.6 and 3.4 m, respectively). VES 30–34 zone is suspected to host a younger furnace F_2 with an adjoining slag trench S_2. The centre of the suspected furnace F_2, is around VES 32 while that of the suspected iron slag trench S_2, is around VES 36. The resistivity profile peaks (P_7 and P_8) around these centres.

Using the same analysis, a much younger furnace F_3 is suspected to be located at the northern edge of the negative anomaly closure A_1 and transits into the positive anomaly zone between VES 8 and 11 with the centre at around VES 10. The suspected adjoining slag trench S_3, is located within VES 6–8 with centre at VES 7. These two centres coincide with peaks P_2 and P_3 along the resistivity profile. Peak P_1 is also likely located over another feature of archaeological interest for which a pronouncement could not be made because of inadequate data. Generally, the average resistivity values of the index layer within zones

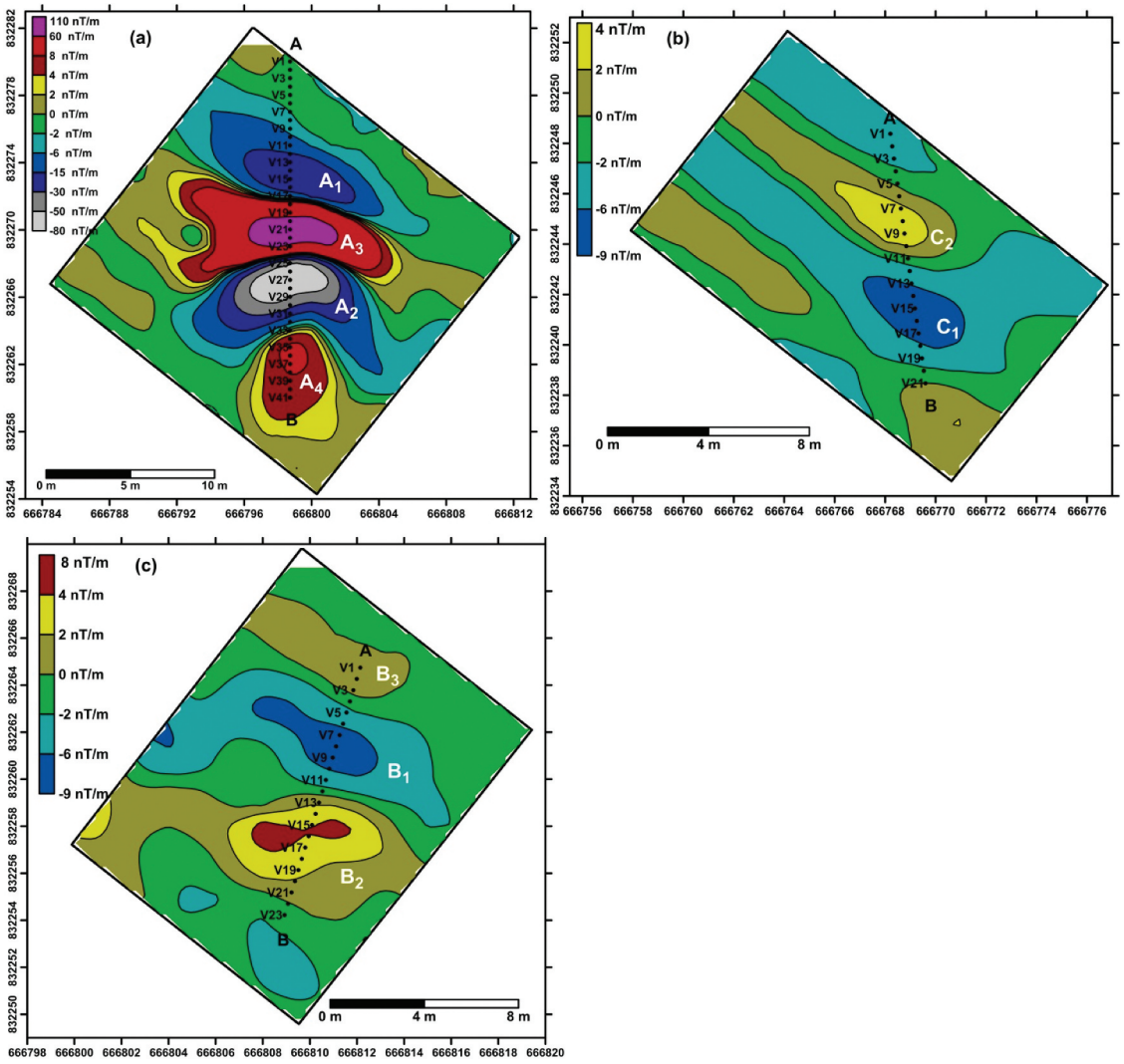

Figure 10. RTE gradient magnetic map of anomalous (a) zone A (site 1) (b) zone B (site 1) (c) zone C (site 2) (Olorunfemi et al. 2021) with superimposed micro VES profile A-B.

suspected to host furnaces are slightly higher than that of the associated slag trenches while the depths of the index horizon are deeper beneath the suspected furnaces than slag trenches.

3.2.2. Site 1 magnetic anomaly zone B

Figure 13(a) (bottom) displays the geoelectric section generated across magnetic anomalous closures B_1 and B_2. The negative anomaly closure B_1 was interpreted as suspected furnace while the positive closure B_2 as slag channel. Three resisto-archaeological layers were delineated beneath this site. The first layer has resistivity values of between 45 and 740 Ωm and thicknesses of between 0.05 and 0.73 m but generally <0.4 m (40 cm). This layer is composed of humus soil, clay, sandy clay and clayey sand. The second (index) layer resistivity values vary from 86 to 238 Ωm (Figure 13(b) (top)) with thicknesses of between 1.6 and 5.3 m. The third layer, which constitutes the bedrock, ranges in resistivity values from 131 to 1326 Ωm and depths to bedrock of 2.3–5.6 m.

The index layer is thickest beneath VES 9 with depth extent of 5.3 m which coincides with index resistivity peak P'_3. This zone VES 8–10 is suspected to host a small furnace F_1, whose slag trench S_1, falls within zone VES 6–8 with centre at VES 7 and resistivity peak P_3 (Figure 13(b)). Resistivity peak P_2, is located at the centre of a 4.8 m thick index horizon suspected to be a younger furnace F_2, whose slag trench S_2, is suspected to be located between VES 2–4 (with centre at VES 3) and index horizon thickness of 4.4 m. The centre coincides with peak P_1. The other resistivity peaks P_4 – P_6 are relatively low resistivity peaks and do not coincide with troughs beneath VES 15 and 19 and hence may not be of resisto-thermal archaeological significance. At this locality, a slag trench is suspected to be located within the negative magnetic anomaly closure B_1.

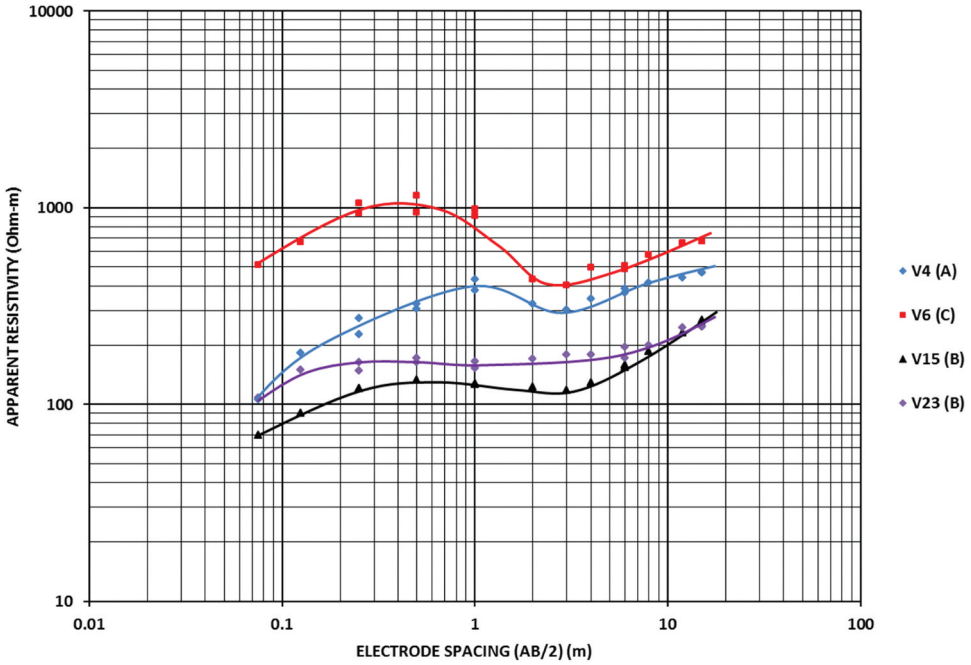

Figure 11. Typical VES curves at OAU iron smelting site.

3.2.3. Site 2 magnetic anomalous zone C

Figure 14(a) shows the geoelectric section developed across magnetic anomalous closures C_1 and C_2. The negative anomaly closure (C_1) was interpreted as a suspected furnace while anomaly closure C_2, as a slag trench. The geoelectric section delineated three resisto-archaeological layers. The first layer has resistivity values ranging from 115 to 6160 Ωm and thicknesses of 0.19–0.63 m but generally less than 0.5 m (50 cm). It is composed of humus soil, sandy clay and laterite. The second and index layer has resistivity values varying from 186 to 442 Ωm (Figure 14(b)) and thicknesses of 0.7–8.4 m. The third layer (bedrock) has resistivity values of between 576 and 1396 Ωm and depths to bedrock of 1.0–8.8 m. The resistivity profile displays five peaks. Peaks P_5 and P_6 (Figure 14(b)) are located over the most prominent zone (VES 14–18) with the highest depth (8.8 m) of index horizon 2. This feature is suspected to be a furnace and falls within and towards the northern edge of the negative magnetic closure C_1 with centre at around VES 15 and an adjoining slag trench peak P_4 (VES 13). Peaks P_2 coincides with another zone with significant depth (4 m) of horizon 2 with centre at around VES 7. This is suspected to be a smaller and younger furnace F_2. Resistivity peak P_1 is located over the adjoining slag (S_2) with centre around VES 4. Suspected furnace F_2, is located at the northern edge of high magnitude positive anomaly closure C_2. Using the depth extent of horizon 2 (8.8 m) at this site as basis, furnace F_1 (at this site 2) might be younger than furnace F_1 at site 1, with a deeper depth of 13 m of the index horizon.

3.3. Inferences

Using the Iyekere geoelectric characteristics of a furnace/slag trench as outlined earlier, the magnetic anomalous zone A (A_1, A_2, A_3, A_4) at site 1 which is suspected, based on magnetic anomalies, to host two furnaces and equal number of associated slag trenches (Table 1), could host as many as three furnaces (F_1, F_2 & F_3) with associated slag trenches (S_1, S_2 & S_3) and even more. The geoelectric results also show that the magnetic anomalous zone B (B_1 & B_2) at site 1 which is suspected to host a furnace and a slag may host as many as two furnaces with adjoining slag trenches. The results also identify one prominent furnace (F_1) and a smaller furnace F_2, and their adjoining slag trenches S_1 and S_2 associated with anomalies C_1 and C_2 at site 2. At the investigated sites 1 and 2, geoelectric results show that furnaces are located within the high amplitude negative polarity magnetic anomaly closures but are slightly shifted off the centre (as observed by Powell et al. (2002)) and straddle into the transition zone between positive and negative amplitude magnetic anomaly closures, while the slag trenches are generally situated within the positive magnetic anomaly closures and almost at the middle or slightly shifted to the edge. If the above inferences are proven by excavation, it could mean, and as observed by Powell et al. (2002), that magnetic anomaly closures are cumulative responses from the magnetic anomalies due to all features within an iron smelting site and may not be that of a distinct feature (e.g. furnace or slag trench) only.

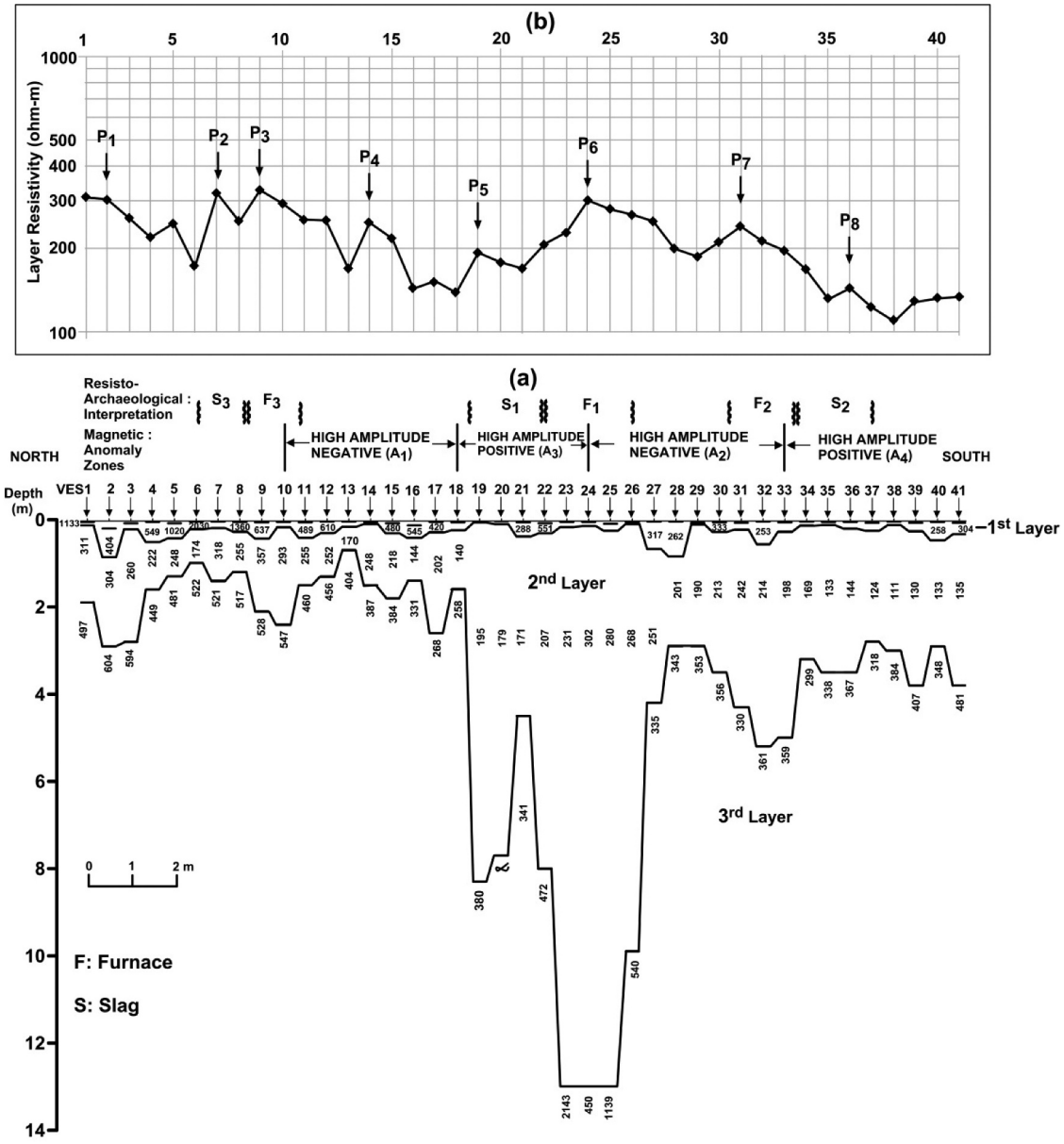

Figure 12. (a) Geoelectric section across magnetic anomalous zone A, site 1 (b) resistivity profile of the index second resisto-archaeological layer.

Based on the geoelectric results, the projected diameter of the suspected furnaces varies from < 1–2 m while the width of the slag channels ranges from 0.5–1 m.

In view of our new findings, a modified archaeological excavation map is developed for site 1 (anomalous zone A) as shown in Figure 15.

4. Preliminary archaeological excavation

A 4 m by 2 m pit was selected for archaeological excavation at site 1 (magnetic anomalous zone A) in the summer of 2019. The excavated area cut across the magnetic interpreted slag trench (high positive magnetic anomaly) and part of the furnace (magnetic low (negative)) anomaly. The site was excavated to a maximum depth of 1.4 m.

Recovered archaeological artefacts are typical of iron smelting site and activities and ranged from iron noodles (tap iron) and slags, tuyere fragments, fired clay/furnace wall fragments, charcoal/ash, potsherds, stones, fragments of a glass bottle, smelted laterite and grey gneiss rock (Figure 16). The pit was terminated on a lateritic horizon (paleo-soil). The archaeological features are baked subsoil sections, channel-shaped burrows and hard/baked furnace floor with consolidated clay mound/charcoal/ash infilling.

The stratigraphic section of the western wall, along a N-S profile, is presented in Figure 17. Consolidated to moderately loose iron slags constitute the first layer up to depth range of 0.3–0.6 m. This layer corresponds to the first resisto-archaeological layer in the

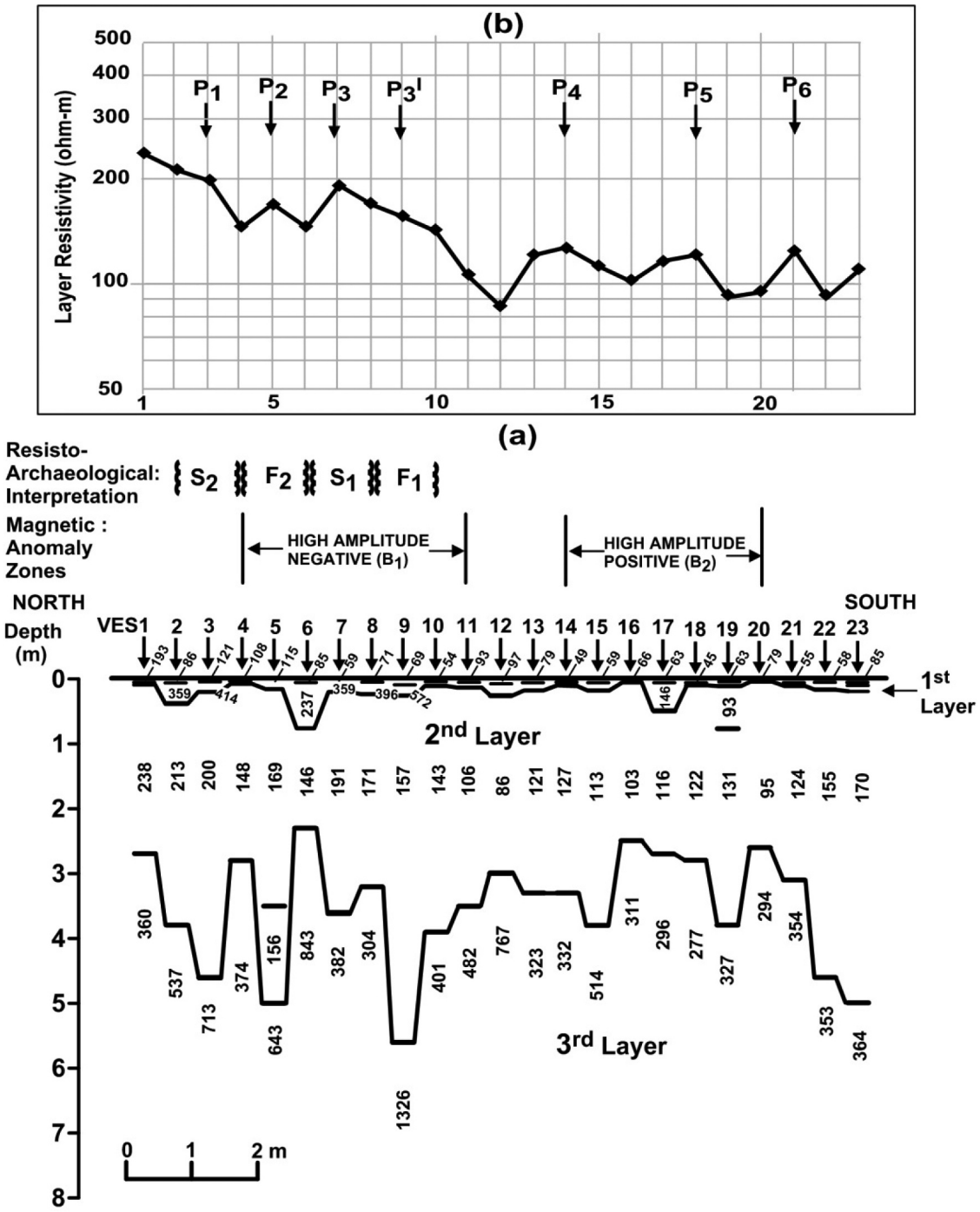

Figure 13. (a) Geoelectric section across magnetic anomalous zone B, site 1 (b) resistivity profile of the index second resisto-archaeological layer.

geoelectric sections (Figures 12–14). Tuyere fragments and very few charcoals were found within the slags. The slags are massive, frothy and less compacted at distances 2.0–4.5 m within the suspected slag trench. Massive charcoal layer underlies the slag layer (within the suspected furnace) at the southern half of the profile. The charcoal base is subsequently underlain, in part, by dark grey baked layer and a burrow. The morphology of the baked layer, most especially between distances 2.0 and 1.0 m, mirrors a bell-shape furnace base. The baked layer is thickest at around the location of a burrow. The cylindrical-shape burrow, where fragments of tuyere were recovered, is suspected to have been created by tuyere pipe from which hot air and slag escape from the base of the furnace (Adeniji 1977; Akinjogbin 2004). This furnace feature is located at a depth range of 0.4–0.5 m. The furnace and the overlying charcoal layer pinch out at the edge of the location where the slags were observed to be massive, frothy and less consolidated. This is suspected to be where the furnace mouth opens into a slag trench identified between VES 18 and 21 with its

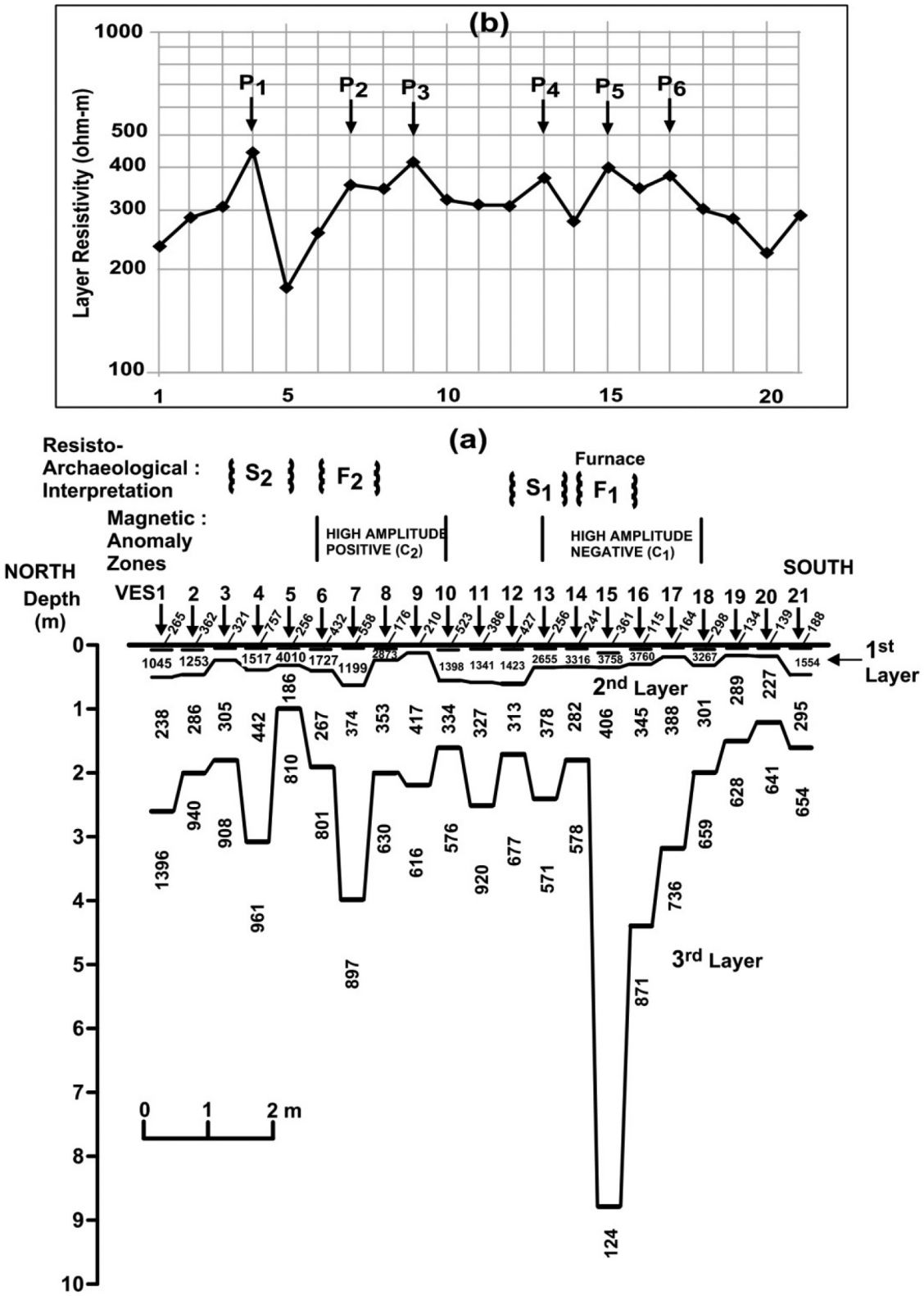

Figure 14. (a) Geoelectric section across magnetic anomalous zone C, site 2 (b) resistivity profile of the index second resisto-archaeological layer.

centre at around VES 19.5 (see Figures 12a and 17). Frothy slags are less dense with the iron component virtually extracted and hence disposed as waste along the slag trench.

Underlying the furnace and the slag trench is a sterile, very dry fine-grained clay soil. The diffusing heat effect from both the furnace and the slag trench could account for the dry nature of this

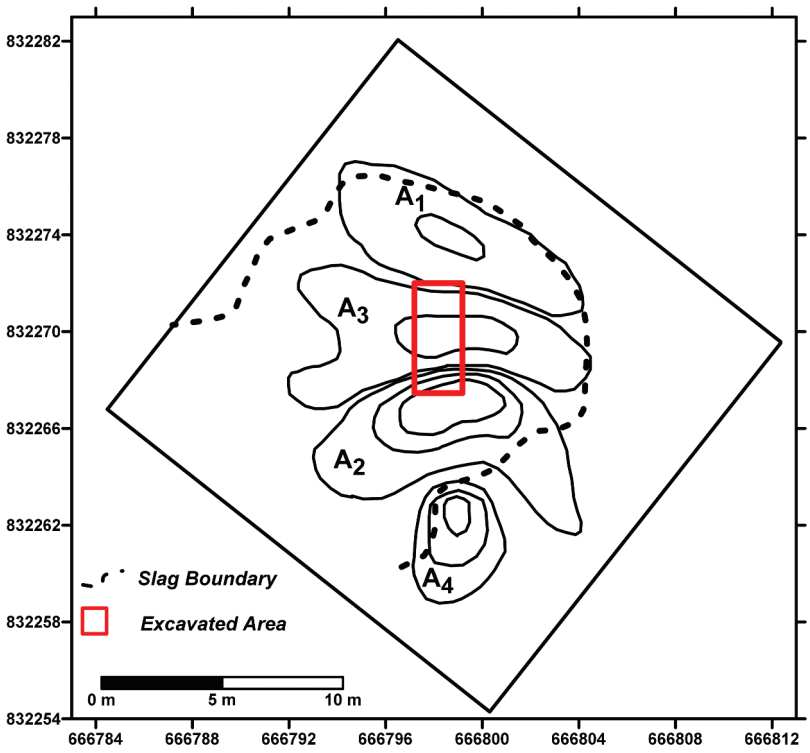

Figure 15. Modified archaeological excavation map for site 1, anomaly zone A.

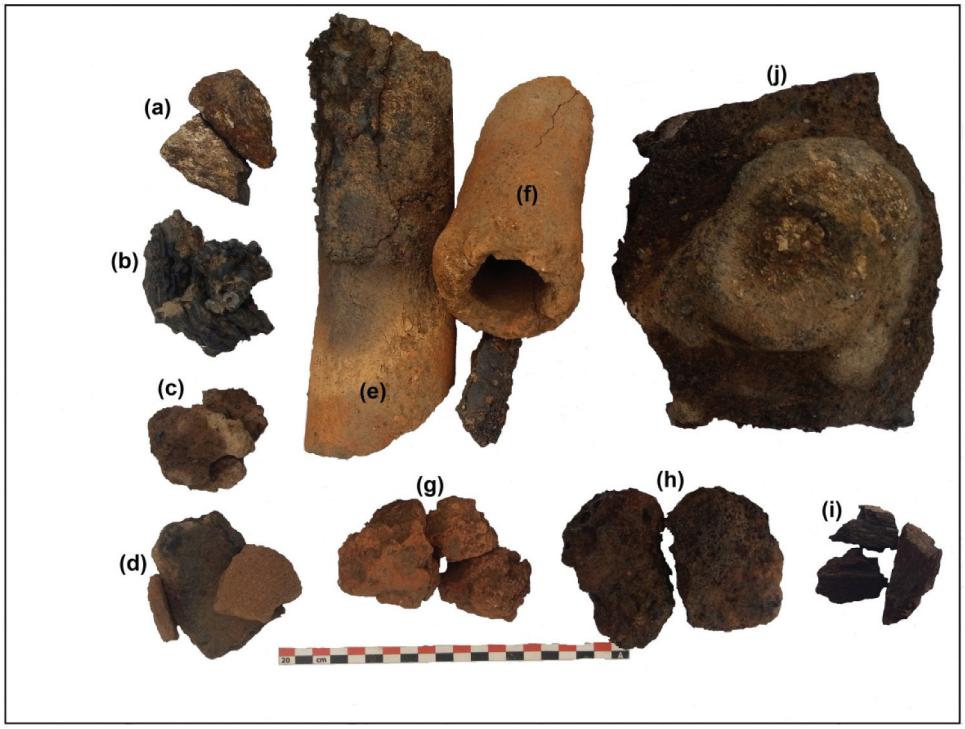

Figure 16. Recovered archaeological artefacts from excavated site 1, anomaly zone A (a) iron stones (b) iron nodules (c) partly smelted laterites (d) potsherds (e) burnt tuyere fragment at the furnace base (f) tuyere pipe (g) relics of furnace wall/fired clay (h) iron slags (i) pieces of charcoal and (j) massive conical-shape iron slag at the base of the furnace.

layer. The sterile layer thins towards the south (the furnace area) where it is underlain, in succession, by gravely stone concretion, moist reddish clay and laterite layers. Lateral continuity of these layers could not be ascertained at the northern half (slag trench) of the pit. Very few charcoals and pot-sherds were recovered from the moist clay layer. Two different cultural occupations were suspected

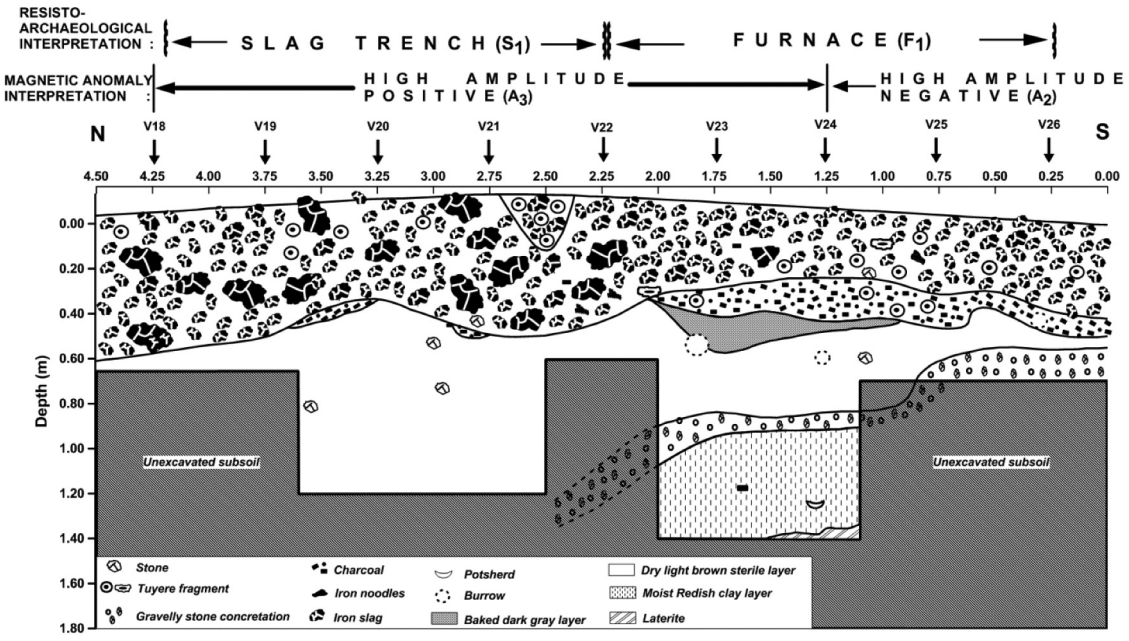

Figure 17. Western wall stratigraphic section of the excavated site 1, anomaly zone A.

within the site. The first is associated with the moist reddish clay while the second is the period of the iron smelting. Both the gravelly stone concretion and the dry sterile clay layers were deposited during the period the site was not occupied.

Charcoals and potsherd from the floor of the furnace and within the moist clay layer were dated using radiocarbon and isotope techniques. Iron smelting activities within the site ranged between 11th and 14th centuries while the first cultural occupation was during 400–700 BC.

5. Discussion and conclusion

The magnetic method remains the most effective reconnaissance geophysical method for the mapping of iron smelting furnace and iron slag channel structures. These archaeological features are characterised by a dipolar magnetic anomaly with the negative polarity anomaly closure, in the low magnetic region, defining the furnace and the positive anomaly closure indicative of the iron slag channel (Powell et al. 2002). However, like in other geophysical methods, these anomalies are much larger in size than the causative bodies, due to edge effect and the bodies are sometimes shifted off the centres of the anomalies (Powell et al. 2002). The precise location of furnaces and associated slag trenches has remained a challenge in the study of ancient iron smelting sites, due to the above interpretation limitations and the fact that most of these archaeological features have been destroyed as a result of infrastructural development and anthropogenic activities, such as mechanised farming. This study has utilised resisto-thermal effect of iron smelting to precisely locate furnaces and iron slag trenches. The methodology involved closely spaced small spacing (micro) Vertical Electrical Sounding across diagnostic dipolar magnetic anomaly closures. The methodology was initially applied to an established ancient iron smelting site (with exposed furnace) at Iyekere, Ile-Ife, to generate geoelectric characteristics (template) for the identification of furnaces/slag trenches. This template was subsequently used to interpret similar geoelectric data from the ancient OAU iron smelting site (Olorunfemi et al. 2021) for which locations of its furnaces and slag channels are unknown due to their obliteration through mechanised agriculture and other anthropogenic activities. From these studies the following geoelectric characteristics evolved.

(i) Enhanced layer resistivity values and depth extent of an index resisto-archaeological layer (the second geoelectric layer) are characteristics of the thermal effect of iron smelting furnace and slag trench.
(ii) The depth extent of the thermal influence on the index layer resistivity beneath the furnace is greater than beneath the iron slag trench; while resistivity profile of the index layer peaks above both the furnace and slag trench.
(iii) The depth extent of the index layer is maximum at around the centre of the furnace and slag trench.
(iv) Where multiple furnaces exist, the depth extents can be used to establish the relative age of the furnaces with older furnaces having greater depth extent of heat impacted index layer.

(v) As observed by Powell et al. (2002), furnace is slightly offset from the centre of the magnetic low (negative), overlapping the transition zone towards the magnetic high (positive) while the slag trench is situated within the magnetic high (positive) zone.

These characteristics and template were used to interpret the geoelectric data from the OAU iron smelting sites 1 and 2. Three suspected furnaces with associated slag channels were identified within anomalous zone A and two suspected furnaces/slag trenches within anomalous zone B, site 1; while two suspected furnaces and associated slag channels were delineated within anomalous zone C at site 2. The suspected furnaces vary in projected diameter from about <1.0–2.0 m while the width of the slag trench ranges from about 0.5–1.0 m.

Preliminary archaeological excavation was carried out on anomalies A_3 and A_2 (between VES stations 17 and 26) at site 1, suspected to host a slag trench and furnace, respectively, from magnetic and geoelectric interpretation (see Figures 12, 15 and 17). Recovered archaeological artefacts typical of an ancient iron smelting site include iron noodles, slags, tuyere fragments, fired clay/furnace wall fragments, charcoal, ash, potsherds, stones, fragments of a glass bottle, smelted laterite and grey gneiss suspected to be raw materials for smelting. Other archaeological features include baked subsoil, channel-shaped burrows and hard/baked furnace floor. These features were identified within a depth range of 0.4–0.5 m.

The baked layer which is diagnostic of the base of the furnace was identified within the furnace – delineated geoelectric zone (VES 22–25) (Figure 12a) with the suspected centre around VES 24. The delineated baked layer falls within VES stations 22.5 and 24.5 (distances 2.0 – 1.0 m) (Figure 17). The geoelectric section identifies the slag trench between VES Stations 18–21 with its centre at around VES 19/20. This zone contains massive and frothy iron slags (see Figure 17). The depth extent of the heat impacted index second layer of the geoelectric section is greater (almost twice as high) than that beneath the slag trench. Expansion of the excavated site in the nearest future will confirm or otherwise the existence of the two additional suspected furnaces/slag trenches (F_2, F_3/S_2, S_3) delineated from the geoelectric data.

Results of the preliminary excavation at site 1 corroborate the archaeological interpretation of the geoelectric section as regards the identification and precise location of the furnace and slag trench structures. It also provided information on the likely diameter and width of the respective features.

It is concluded that a methodology involving detailed close spacing (micro) Vertical Electrical Sounding is effective in precisely locating furnaces/slag trenches at the OAU iron smelting site; and could be applied in areas with similar geologic setting.

Disclosure statement

No potential conflict of interest was reported by the author(s).

ORCID

Martins Olusola Olorunfemi http://orcid.org/0000-0003-3494-3333
Ademakinwa George Oni http://orcid.org/0000-0003-0627-7820

References

Abrahamsen N, Jakobsen PF, Voss O 1984 Archaeology and geophysical prospecting. Working paper No. 14, Nat. Museum of Denmark, Copenhagen, 109–144.
Adeniji D 1977. Iron mining and smelting in Yorubaland. Inst. African Studies, University of Ibadan (occasional publication, no. 31, originally written in Yoruba and translated into English Language by Professor R.G. Armstrong).
Akinjogbin IA. 2004. The impact of iron in Yorubaland. In: Bocoum H, editor. The origins of iron metallurgy in Africa: new light on its antiquity. West and Central Africa: UNESCO Publication 55–61 .
Childs ST. 2000. Traditional iron working: a narrated ethnoachaeological example: in ancient African metallurgy-The socio-cultural context (Edited by. Vogel JO). Walnut Creek (CA): Altamira Press; p. 199–254.
de Barros P. 2000. In: Vogel JO, Edited by. Iron metallurgy: sociocultural context: in ancient African metallurgy-The socio-cultural context. Vol. 94596. Walnut Creek (CA): Altamira Press; p. 199–254.
Deme A, McIntosh SK. 2006. Excavation at Walaide. New light on the settlement of the Middle Senegal valley by iron using peoples. J Afr Archaeol. 4(2):317–347. doi:10.3213/1612-1651-10078.
Fluzin P. 2007. Les analyses metallographiques. In: Zangato E, editor. Les ateliers d'oboui: prenueres Communautes' me'tallurgistes' dans le nord-ouest du centrafriques. Paris: Recherches Sur les civilisations; p. 60–67.
Holl AFC. 2009. Early West African metallugies: new data and old orthodoxy. Journal of World Prehistory. 22 (4):415–438. doi:10.1007/s10963-009-9030-6.
Ige A, Rehren T. 2003. Black sand and iron stone: iron smelting in Modakeke, Ife, Southwestern Nigeria. IAMS. 23:15–20.
Jemkur JF. 2004. The beginnings of iron metallurgy in West Africa. In: Bocoum H, editor. The origin of iron metallurgy in Africa: new light on the antiquity. West and Central Africa: UNESCO Publication 33–42 .
Kozhevnikov NO, Kharinsky AV, Snopkov SV. 2018. Geophysical prospection and archaeological excavation of ancient iron smelting sites in the Barun-Khal valley on the western shore of lake Baikal (Olkhon region, Siberia). Archaeol Prospect 1–17. doi:10.1002/arp.1727. wileyonlinelibrary.com/journal/arp

Okafor EE. 2002. La re'duction du fer dans les Bas-Four neaux-une industrie Vieille de 2500 ans au Nigeria. In: Bocoum H, editor. Aux origines de la me'tallugrgie du fer en Afrique. Paris: Editions UNESCO; p. 35–48.

Olorunfemi MO, Ogunfolakan BA, Oni AG, Fadare TK, Bamidele OE. 2021. On the application of geophysics in archaeology: case study, OAU Ile-Ife, iron smelting site, Southwest Nigeria. In: Kehinde A, Aremu O, and Nton M, editors. Homage for a gentleman scholar-administrator: a festschrift in honour of Professor Abel Idowu Olayinka. Ibadan, Nigeria: Printing Press University of Ibadan; Chapter 28, p. 373–405.

Oyeyemi KO, Oladunjoye MA, Olayinka AI, Aizebokhai AP. 2015. Geophysical imaging of archaeological materials at Iyekere, Ile-Ife, Southwestern Nigeria. J Environ Earth Sci. 5(2):148–157.

Pattantyús-Á M. 1986. Geophysical results in archaeology in Hungary. Geophysics. 51(3):561–567. doi:10.1190/1.1442110.

Powell AJ, McDonnell JG, Batt CM, Vermon RW. 2002. An assessment of the magnetic response of an iron-smelting site. Archaeometry. 44(4):651–665. doi:10.1111/1475-4754.00091.

Reynolds JM. 1997. An introduction to applied and environmental geophysics. England: John Wiley and Sons Ltd.

Sharma PV. 1997. Environmental and engineering geophysics. Cambridge: Cambridge University Press; p. 105–109.

Telford WM, Geldart LP, Sheriff RE. 1990. Applied geophysics. second ed. Cambridge: Cambridge University Press.

Appendix

Table A1. Iyekere iron smelting site VES interpretation results.

VES	$D_1, D_2, D_3 \ldots\ldots\ldots D_n$	$\rho_1, \rho_2, \rho_3 \ldots\ldots\ldots\ldots\ldots \rho_n$	Type Curve
1	0.05/0.08/0.14/1.3/3/6.1/15	201/111/1099/136/67/202/57/∞	HKQHKH
2	0.04/0.12/0.29/0.95/2.8/5.6	121/456/92/186/113/185/85	KHKHK
3	0.05/0.18/3.1/13.0	182/500/168/98/22	KQQ
4	0.18/0.34/3.7/14.0	231/253/126/81/886	KQH
5	0.1/0.14/0.26/4.7/15.0	365/443/422/153/105/259	KQQH
6	0.03/0.07/0.29/3.2/4.5/16.0	649/173/453/174/296/128/1052	HKHKH
7	0.02/0.09/0.25/2.2/4.3/12.0	319/96/448/83/242/90/281	HKHKH
8	0.21/0.25/0.57/4.5/5.9/14.0	155/110/338/112/147/129/352	HKHKH
9	0.04/0.08/0.33/4.8/6.8	139/120/196/116/213/100	HKHK
10	0.03/0.08/0.2/8.0/10.0	515/118/462/109/222/65	HKHK
11	0.04/0.35/8.0	509/220/128/58	QQ
12	0.04/0.08/0.78/2.2/7.0	332/1155/178/71/172/41	KQKH
13	0.1/0.15/0.21/1.3/5.2/8.8	162/293/1360/61/232/16/∞	AKHKH
14	0.09/0.19/0.44/1.7/6.1	240/181/193/76/297/18	HKHK
15	0.04/0.62/1.5/3.8/7.7	442/111/34/322/20/329	QHKH
16	0.12/2.1/3.3/3.7	178/79/355/706/50	HAK
17	0.06/0.29/0.75/2.4/8.5	187/92/33/209/43/∞	QHKH
18	0.06/1.0/1.8/11.0	213/75/135/76/∞	KHK
19	0.05/0.26/0.53/1.5/2.4/9.1	420/82/169/96/145/58/∞	HKHKH
20	0.07/0.27/4.6/12.0	75/405/110/168/26	KHK
21	0.03/0.14/0.51/6.1	772/104/441/160/284	HKH
22	0.03/0.07/0.42/1.7	412/98/544/98/195	HKH
23	0.02/0.05/0.5/1.7/4.4	1502/94/474/88/570/187	HKHK
24	0.06/0.11/0.33/6.4/9.7	262/207/511/181/347/104	HKHK
25	0.09/0.12/0.47/4.6/6.1	189/186/277/132/457/110	HKHK
26	0.03/0.11/0.37/1.5	435/139/663/69/291	HKH
27	0.05/0.13/0.76/8.2	217/647/234/157/86	KQQ

D: Depth (m); ρ: Layer Resistivity (ohm-m)

Table A2. OAU iron smelting site VES interpretation results – site 1, anomaly zone A.

VES	$D_1, D_2, D_3 \ldots\ldots\ldots D_n$	$\rho_1, \rho_2, \rho_3 \ldots\ldots\ldots\ldots\ldots \rho_n$	Type Curve
1	0.05/0.13/1.9	104/1133/311/497	KH
2	0.2/0.86/2.9	280/404/304/604	KH
3	0.08/0.22/2.8	133/839/260/594	KH
4	0.05/0.51/1.6	82/549/222/449	KH
5	0.08/0.43/1.3	120/1020/248/481	KH
6	0.04/0.21/0.99	53/2032/174/522	KH
7	0.04/0.19/1.4	83/1491/318/521	KH
8	0.05/0.27/1.2	116/1360/255/517	KH
9	0.06/0.43/2.1	176/637/357/528	KH
10	0.05/0.17/2.4	143/761/293/547	KH
11	0.06/0.41/1.5	209/489/255/460	KH
12	0.04/0.31/1.3	132/610/252/456	KH
13	0.04/0.16/0.69	74/1346/170/404	KH
14	0.04/0.09/1.5	158/854/248/387	KH
15	0.08/0.31/1.8	252/480/218/384	KH
16	0.13/0.41/1.4	166/545/144/331	KH
17	0.05/0.28/2.6	198/420/202/268	KH
18	0.06/0.24/1.6	56/452/140/258	KH
19	0.05/0.06/8.3	86/620/195/380	KH
20	0.03/0.1/7.7	88/545/179/∞	KH
21	0.06/0.38/4.5	129/288/171/341	KH
22	0.08/0.31/8.0	103/551/207/472	KH
23	0.05/0.17/13.0	59/1037/231/2143	KH
24	0.05/0.14/13.0	76/956/302/450	KH
25	0.09/0.25/13.0	115/1189/280/1139	KH
26	0.05/0.1/9.9	57/1025/268/540	KH
27	0.04/0.67/4.2	122/317/251/335	KH
28	0.04/0.84/2.9	90/262/201/343	KH
29	0.07/0.1/2.9	165/248/190/353	KH
30	0.06/0.28/3.5	154/333/213/356	KH
31	0.07/0.23/4.3	126/393/242/330	KH
32	0.04/0.56/5.2	96/253/214/361	KH
33	0.06/0.27/5.0	71/412/198/359	KH
34	0.04/0.13/3.2	38/1155/169/299	KH
35	0.05/0.12/3.5	87/440/133/338	KH
36	0.05/0.2/3.5	59/551/144/367	KH
37	0.07/0.25/2.8	84/483/124/318	KH
38	0.04/0.12/3.0	42/845/111/384	KH
39	0.07/0.26/3.8	107/443/130/407	KH
40	0.05/0.47/2.9	44/258/133/348	KH
41	0.07/0.33/3.8	83/304/135/481	KH

Table A3. OAU iron smelting site VES interpretation results – site 1, anomaly zone B.

VES	$D_1, D_2, D_3 \ldots\ldots\ldots D_n$	$\rho_1, \rho_2, \rho_3 \ldots\ldots\ldots\ldots\ldots \rho_n$	Type Curve
1	0.04/0.08/2.7	193/849/238/360	KH
2	0.05/0.38/3.8	86/359/213/537	KH
3	0.04/0.2/4.6	121/414/200/713	KH
4	0.04/0.08/2.8	108/674/146/374	KH
5	0.19/3.5/5.0	115/169/156/643	KH
6	0.05/0.73/2.3	85/237/146/843	KH
7	0.03/0.2/3.6	59/386/191/382	KH
8	0.05/0.22/3.2	71/396/171/304	KH
9	0.09/0.25/5.6	69/572/157/1326	KH
10	0.04/0.09/3.9	54/740/143/401	KH
11	0.05/0.13/3.5	93/380/106/482	KH
12	0.08/0.25/3.0	97/190/86/767	KH
13	0.06/0.18/3.3	79/237/121/323	KH
14	0.05/0.1/3.3	49/600/127/332	KH
15	0.06/0.19/3.8	59/209/113/514	KH
16	0.04/0.07/2.5	66/469/103/311	KH
17	0.05/0.49/2.7	63/142/116/296	KH
18	0.05/0.1/2.8	45/372/122/277	KH
19	0.04/0.11/0.77/3.8	63/249/93/131/327	KHA
20	0.04/0.05/2.6	79/361/95/294	KH
21	0.05/0.1/3.1	55/148/124/354	KH
22	0.04/0.06/0.15/4.6	58/701/93/155/353	KHA
23	0.05/0.09/0.19/5.0	85/436/110/170/364	KHA

Table A4. OAU iron smelting site VES interpretation results – site 2, anomaly zone C.

VES	$D_1, D_2, D_3 \ldots\ldots\ldots D_n$	$\rho_1, \rho_2, \rho_3 \ldots\ldots\ldots\ldots\ldots \rho_n$	Type Curve
1	0.07/0.5/2.6	265/1045/238/1396	KH
2	0.07/0.47/2.0	362/1253/286/940	KH
3	0.04/0.23/1.8	321/3232/305/908	KH
4	0.05/0.41/3.1	757/1517/442/961	KH
5	0.05/0.3/1.0	256/4010/186/810	KH
6	0.06/0.41/1.9	432/1727/267/801	KH
7	0.05/0.63/4.0	558/1199/374/897	KH
8	0.05/0.26/2.0	176/2878/353/630	KH
9	0.04/0.13/2.2	210/6160/417/616	KH
10	0.07/0.56/1.6	523/1398/334/576	KH
11	0.04/0.58/2.5	386/1341/327/920	KH
12	0.07/0.6/1.7	427/1423/313/677	KH
13	0.05/0.33/2.4	256/2655/378/571	KH
14	0.06/0.36/1.8	241/3316/282/578	KH
15	0.12/0.36/8.8	361/3758/406/1241	KH
16	0.05/0.3/4.1	115/3760/345/871	KH
17	0.04/0.19/3.2	164/5223/388/736	KH
18	0.08/0.33/2.0	298/3267/301/659	KH
19	0.04/0.16/1.5	134/5857/289/628	KH
20	0.04/0.19/1.2	139/5058/227/641	KH
21	0.04/0.46/1.6	188/1554/295/654	KH